A Pseudo-Spectral Approach for the Incompressible Boundary Layer Equations with Automatic Normal Scaling

by M. Storti

Grupo de Tecnología Mecánica del INTEC
Güemes 3450, 3000 - Santa Fe, Argentina
Phone/Fax: 54-42-55.91.75, Fax: 54-42-55.09.44
e-mail: mstorti@minerva.unl.edu.ar
home-page: http://venus.unl.edu.ar/gtm-eng.html

File: blay3d4.tex

$Id: blay3d4.tex,v 1.7 1998/06/26 15:21:47 mstorti Exp $

Keywords

- boundary layer equations
- spectral methods
- meshless methods
- viscous flow
- incompressible flow
- laminar flow
- parabolized Navier-Stokes equations

Running title

Spectral Approach to Boundary Layer Equations

What are the boundary layer equations?

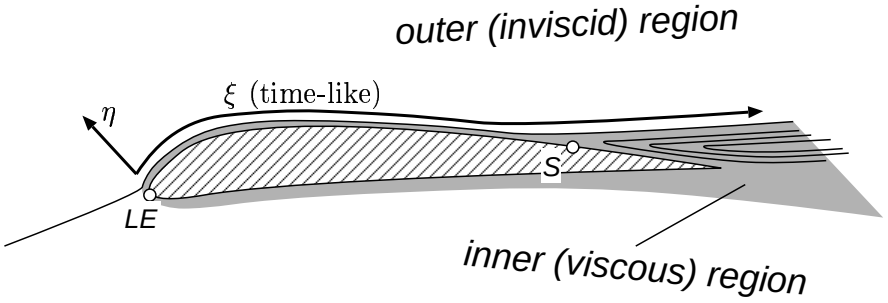

Figure 1: (File: outer)

- For exterior high Reynolds number flows, the flow can be decomposed in an exterior *inviscid region* and an interior *viscous region*. A natural way to solve this is to solve the inviscid equations (potential, Euler) in the exterior region and *Parabolizad Navier-Stokes Equations* in the inner region.
- Parabolized Navier-Stokes Equations amounts essentially to neglect diffusive terms in the longitudinal direction. This allows to solve the equations as if the longitudinal coordinate were time-like. Thus, computational resources (CPU-time, core memory) are highly reduced.
- Boundary layer problems are the paradigm of *singular perturbation problems*. Other problems that can be solved with this formulation are:
  - ▷ WKB theory for wave like problems (Helmholtz equations) in the limit of short wave-lengths (optical limit)
  - ▷ Rounded leading edges

Typical inviscid/boundary layer calculation

- Compute the inviscid field with slip condition at the wall.
- Solve the boundary layer problem with the inviscid values at the wall as input data.
- Compute the displacement thickness.
- Solve again the inviscid problem with a geometry enlarged by the displacement thickness. This can be done by modifying the geometry or simulated by injecting fluxes at the wall.
- Repeat the process until convergence.

This process converges, unless very strong separation is present in the flow field.

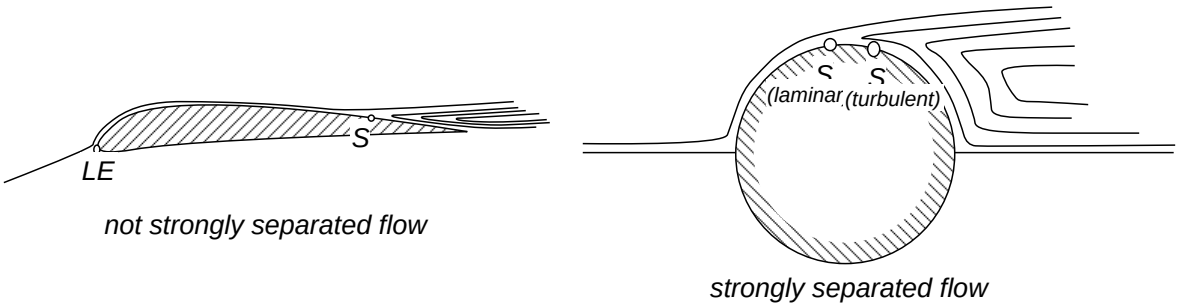

Figure 2: (File: separat)

Why to solve the boundary layer equations?

Even if nowadays the solution of NS equations on full configurations is possible on workstations or networks of workstations, very cheap solvers as inviscid/boundary layer solutions are wanted specially when many, many solutions (iteration) of the problem are needed. For instance:

- Shape optimization
- Free surface problems with very different time scales
- Computation of flows for a full family of parameters (Froude number in ship hydrodynamics.)

Nowadays b.l. eqs. are solved mainly with..

- Integral methods. (Non-convergent. Mainly in the aeronautical design).
- Finite differences.
- Finite elements (less used. See Schetz, Hytopoulos & M. Gunzburger FED-vol 123, Advances in Finite Element Analysis in Fluid Dynamics, ASME (1991)
- Spectral methods for high precission computations. Hydrodynamical stability of the boundary layer. (Pruett & Streett, International Journal for Numerical Methods in Fluids , **13**, pp. 713-737 (1991))

Contributions of this work

- Automatic scaling of the normal coordinate
- Spectral discretization in the normal coordinate and mesh-less discretization in the surface coordinates (3D).
- New mapping for the normal coordinate (avoids unnecessary refinement at the outer edge).
- Tensorial form of the b.l. eqs.

Automatic scaling of the normal coordinate

The incompressible laminar 2D boundary layer equations are:

$$\begin{aligned} u u_{,x} + v u_{,y} &= \nu\, u_{,yy} + U_{\text{ext}} U_{\text{ext},x} \\ u_{,x} + v_{,y} &= 0 \end{aligned} \qquad \text{(1.a,b)}$$

The boundary layer thickness δ may greatly vary. It grows like $\sqrt{x}$ for flat velocity profiles, and gets very thin for highly accelerated flows, like in the region near the suction peak of aero foils. For accuracy reasons it is highly desirable to keep the width of the computational domain (roughly) close to the b.l. thickness.

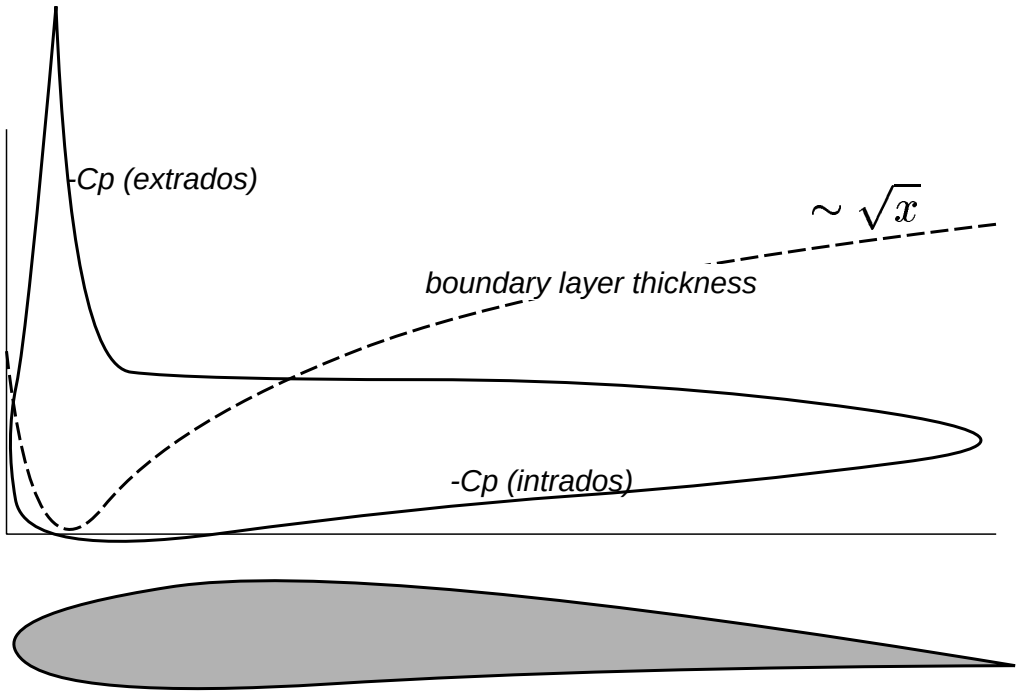

Figure 3: (File: blgrow)

Introducing an arbitrary normal scaling length δ_{scal} we get the transformed equations:

$$\begin{aligned} U U_{,\xi} + V U_{,\eta} &= \frac{\nu}{{\delta_{\text{scal}}}^2} U_{,\eta\eta} + U_{\text{ext}} U_{\text{ext},\xi} \\ \frac{1}{\delta_{\text{scal}}} \left(\delta_{\text{scal}} U\right)_{,\xi} + V_{,\eta} &= 0 \end{aligned} \qquad \text{(2.a,b)}$$

Automatic scaling means to choose $\delta_{\text{scal}} = \delta^*$ and solving the resulting DAE system (Differential Algebraic Equations) appropriately.

Automatic scaling of the normal coordinate *(continued...)*

If we have an *a priori* estimate to the b.l. thickness δ^* then we can use it for scaling purposes, for instance

$$\delta_{\text{scal}} \propto {U_{\text{ext}}}^{-1}(\int U_{\text{ext}}(x)\ dx)^{1/2} \qquad \text{(Levy-Lees transf.)} \quad (3)$$

$$\delta_{\text{scal}} = \theta_{\text{Thwaites}} \propto \left(\frac{1}{U_{\text{ext}}^6}\int U_{\text{ext}}^5\ dx\right)^{1/2} \qquad \text{(Thwaites method)} \quad 4)$$

These give correct behavior $\delta_{\text{scal}} \propto x^{1/2(1-m)}$ for wedge flows ($U_{\text{ext}} \propto x^m$).

However, large discrepancies exist in the location of the separation point.

After semi-discretization in the normal coordinate (by spectral methods or whatever) we get a system of ODE's of the form

$$\mathbf{F}(\mathbf{a}, \delta_{\text{scal}}, \dot{\mathbf{a}}, \dot{\delta}_{\text{scal}}, x) = 0 \tag{5}$$

where $\mathbf{a}$ is the vector of unknowns defining the b.l. profile.

$$u(x,\eta) = U_{\text{ext}}(x)\ \left(\sum_k a_k(x)\phi(\eta)\right) \tag{6}$$

Imposing exactly $\delta_{\text{scal}} = \delta^*$ amounts to a further linear restriction on the a_k's.

$$U_{\text{ext}}\delta^* = \int_0^\infty (U_{\text{ext}} - u)\ dy \tag{7}$$

$$1 = \int_0^\infty (1 - u/U_{\text{ext}})\ d\eta = \sum_{k=0}^{M} \beta_k\, a_k \tag{8}$$

Auto-scaling amounts to solve (5) together with restriction (8). These represents a DAE's (Differential Algebraic Equations) system. Two possibilities arise

- Eliminate δ_{scal} and obtain a ODE's system.
- Use a special purpose package for DAE's like DASSL (Brenan), LIMEX (Nowak & Zugck).

Spectral discretization

- Spectral methods are based on approximation by non-local functions, and (under certain conditions) give very high convergence rates (fast than any finite power of the number of unknowns). This is known as *spectral convergence*.
- The simplest example is Fourier series for problems with periodic conditions.
- For finite intervals (say $0 < x < 1$) one can transform the problem to a in periodic by mapping $x = \frac{1}{2}(1 - \cos\theta)$. This is equivalent to Tchebyschev polynomial expansion.

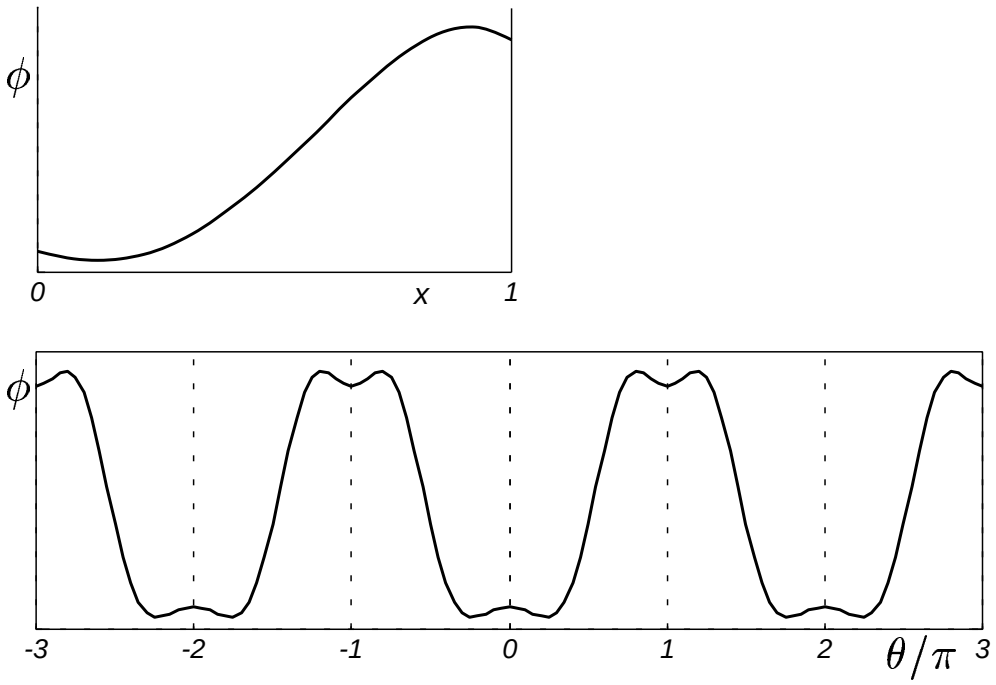

Figure 4: (File: gmap)

Spectral discretization *(continued...)*

- For semi-infinite intervals (as is the case for the b.l. equations) it's usual to truncate the domain, say $0 < \eta < \eta_{\max}$ and then apply the Tchebyschev expansion. This results in an undesired refinement near the outer boundary.

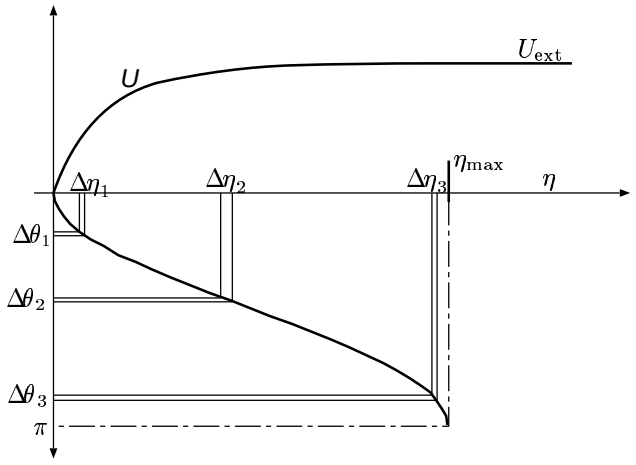

Figure 5: (File: etares)

- To correct this we propose the following mapping, which gives a uniformly decreasing resolution from the wall to the outer edge of the b.l.

$$\tanh\left(\frac{\eta}{\eta_{\text{scal}}}\right) = \left[\tfrac{1}{2}(1-\cos\theta)\right]^2 \tag{9}$$

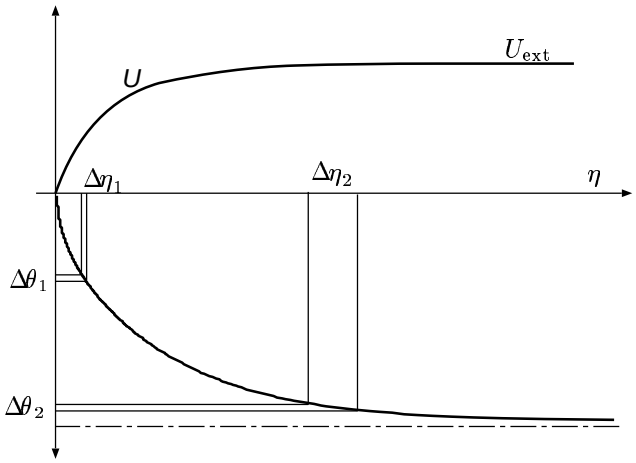

Figure 6: (File: etarestanh)

1. Tensorial form of the b.l. eqs.

It is obvious that some kind of *intrinsic curvilinear coordinates* $(\xi, \eta) = (x_1, x_2)$ are needed on the surface. Let $\zeta = x^3 = n/\delta(x_1, x_2)$ be the normal coordinate to it. Navier-Stokes equations in a general 3D curvilinear system are written in the following form:

$$\begin{aligned} u^i \, u^j_{,i} &= \nu u^j_{,ii} + g^{ji} p_{,i} \\ u^i_{,i} &= 0 \end{aligned} \tag{10}$$

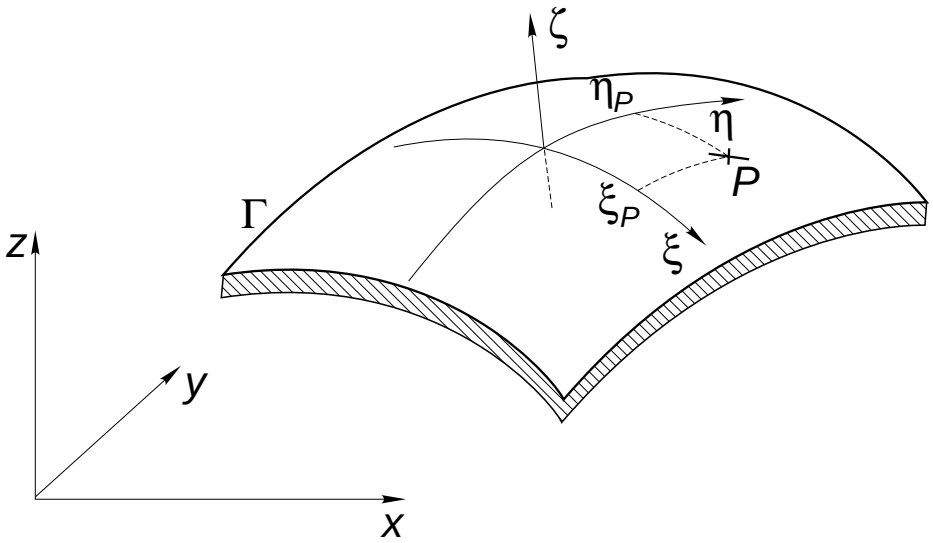

Figure 7: intrinsic coordinates on a surface(File: ../EPS/intri)

- Upper (lower) subscripts denote *"contravariant"* (*"covariant"*) components of the vectors or tensors.
- $(\,)_{,i}$ denotes the *"covariant derivative"*, where the 3-index term in braces is the Christoffel symbol:

$$u^i_{,j} = \frac{\partial u^i}{\partial x_j} + \left\{ \begin{matrix} i \\ j \; k \end{matrix} \right\} u^k \tag{11}$$

Boundary layers in tensorial form *(continued...)*

The following "beasts" arise in the context of tensorial calculus:

- *Christoffel symbols of second kind*:

$$\left\{ \begin{array}{c} i \\ j\ k \end{array} \right\} = g^{ip}\,[jk,p] \tag{12}$$

- *Christoffel symbols of first kind*:

$$\begin{aligned} [jk,q] &= \sum_p \frac{\partial^2 y^p}{\partial x_j \partial x^k}\frac{\partial y^p}{\partial x^q} \\ &= \tfrac{1}{2}\left\{ \frac{\partial g_{qj}}{\partial x^k} + \frac{\partial g_{qk}}{\partial x^j} - \frac{\partial g_{jk}}{\partial x^q} \right\} \end{aligned} \tag{13}$$

- *Contravariant metric tensor*:

$$\mathbf{g}^{\cdot\cdot} = (\mathbf{g}_{\cdot\cdot})^{-1} \tag{14}$$

- *Covariant metric tensor*;

$$(\ ds)^2 = g_{jk}\ dx^j\ dx^k \tag{15}$$

- *Compact form of the continuity equation:*

$$u^i_{,i} = \frac{1}{g^{1/2}}\frac{\partial}{\partial x^i}(g^{1/2}u^i) \tag{16}$$

2. Boundary layers in tensorial form

Letting $\delta \to 0$:

$$\left\{ \begin{array}{l} w\dfrac{\partial u^\beta}{\partial \zeta} + u^\alpha u^\beta{}_{,\alpha} + g^{\beta\alpha}\dfrac{\partial p}{\partial x^\alpha} = \dfrac{\nu}{\delta_s^2}\dfrac{\partial^2 u^\beta}{\partial \zeta^2} \\ \dfrac{\partial w}{\partial \zeta} + \dfrac{1}{\delta_s a^{1/2}}\dfrac{\partial}{\partial x^\alpha}(\delta_s a^{1/2}\,u^\alpha) = 0 \end{array} \right. \tag{17}$$

This eqs. are invariant under change in intrinsic coordinates $(x^1,x^2) \to (w^1,w^2)$ and in transversal scaling: $\delta_s(x^1,x^2)$ is arbitrary.

3. Advantages of writing the b.l. eqs. in tensorial form

- It's easier to detect errors.

  Example: Steady heat conduction equation in a hollow shell

$$\begin{aligned} &(t\, g^{\alpha\beta}\, T_{,\beta})_{,\alpha} = Q \\ &\frac{\partial}{\partial x^{\alpha}}(t\, g^{\alpha\beta}\, a^{1/2}\, \frac{\partial T}{\partial x^{\beta}}) = a^{1/2}\, Q \end{aligned} \tag{18}$$

- Conservative equations remain conservative:

$$f^{i}_{,i} = Q$$

$$\int F^{i}\, dS_{,i} = \int Q\, d\Omega \tag{19}$$

- It's easier to change from one coordinate system to another.
- ***Surface equations are essentially different to space equations: Space is Euclidean, surfaces are (in general) not.***
- Arbitrary scaling of the transverse coordinate is included.

Numerical results. Wedge flow (Hartree profiles)

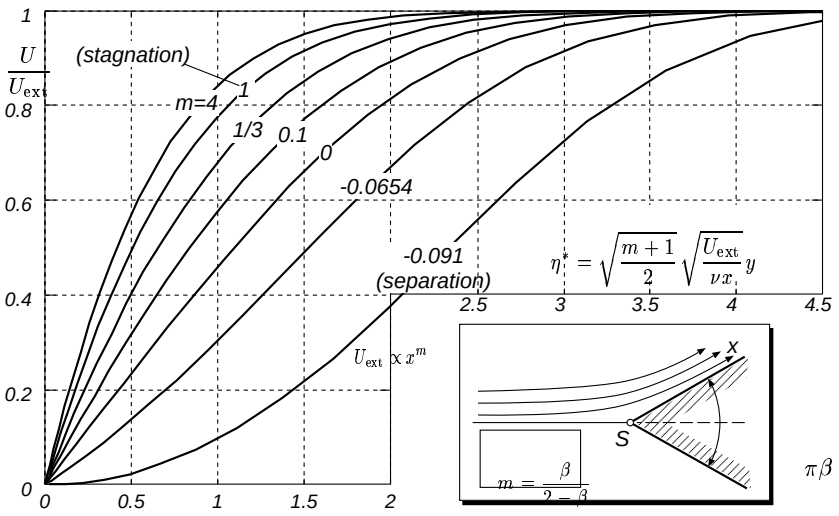

Figure 8: (File: wedgeprof)

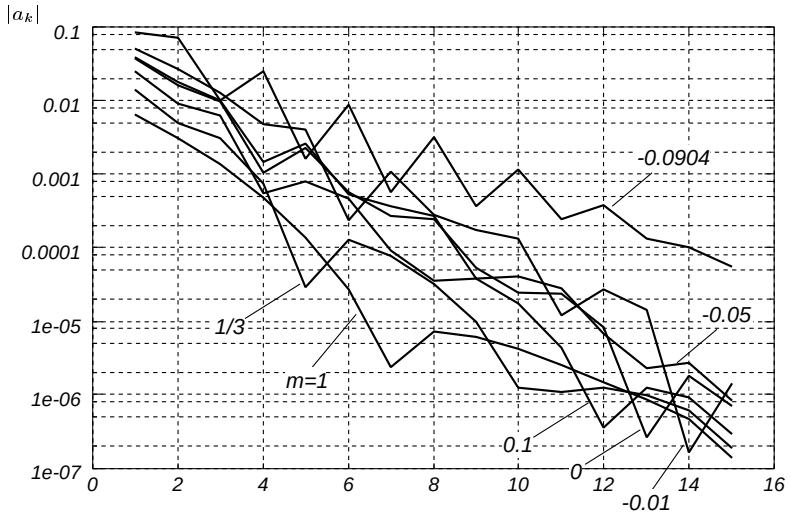

Figure 9: Spectra of coefficients in the Fourier series for similar flows. (File: spectra)

- Good convergence ($< 1\%$) is obtained even with 4 terms (equivalent to the von Kármán and Pohlhausen method).
- Spectral decay of the coefficients means "spectral convergence".

Numerical solutions. Convergent channel

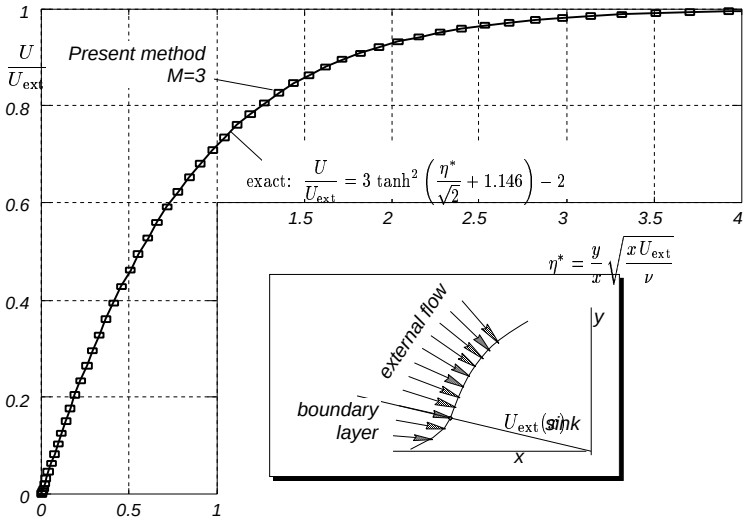

Figure 10: Flow in a convergent channel $U_{\rm ext} \propto |x|^{-1}$, *(*$x < 0$*)*(File: convchan)

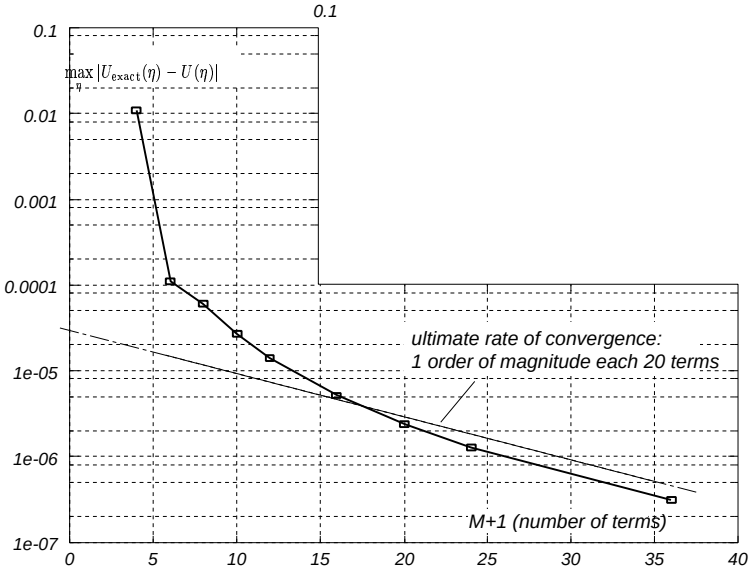

Figure 11: Maximum error versus number of terms for the convergent channel flow ($U_{\rm ext} \propto -|x|^{-1}$*, for* $x < 0$*).* (File: converg)

- Wedge flows have an exact solution for $m = -1$
- The velocity profile obtained with 4 terms is compared here with the exact solution.

Howarth decelerated flow

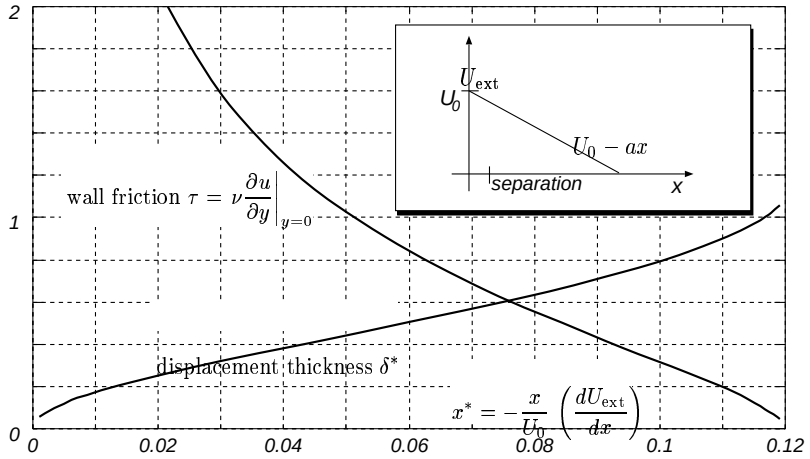

Figure 12: Displacement thickness and wall friction for Howarth's flow $U_{\text{ext}}(x) = U_0 - ax$ (File: howdelta)

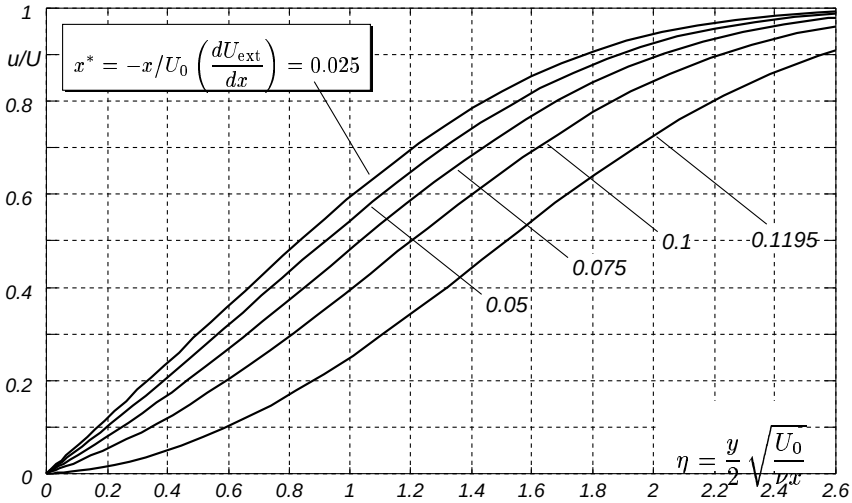

Figure 13: Longitudinal velocity profiles for Howarth's flow. (File: howprof)

- This is also referred as *"linearly retarded flow"*.
- Flow separates at $x^* = 0.01195$ which is in very good coincidence with both the value of $x^* = 0.0119863$ reported by Wippermann.

Ellipses

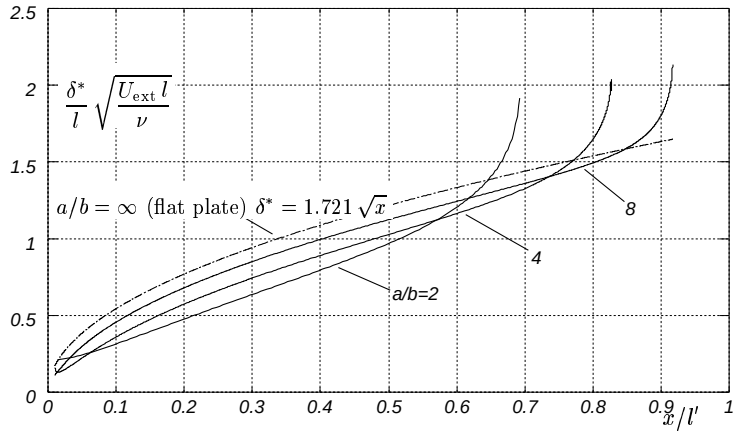

Figure 16: Displacement thickness for flow around ellipses of various slenderness.(File: elipsed)

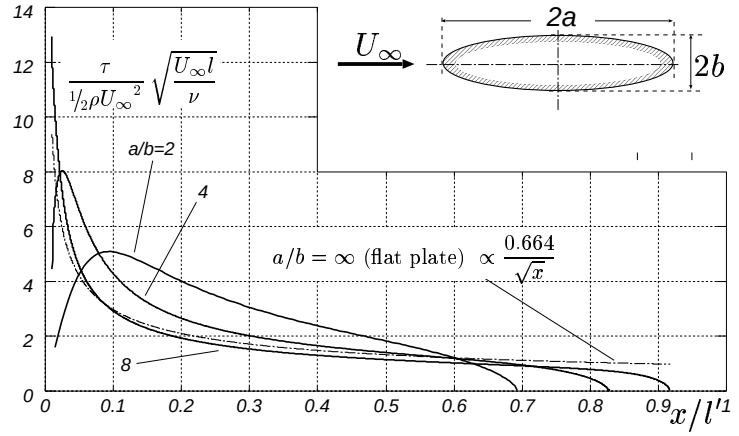

Figure 17: Wall friction or flow around ellipses of various slenderness(File: taueli)

- Displacement thicknesses and wall friction are shown for several aspect ratios.
- The separation point moves to the trailing edge as the aspect ratio $a/b \to \infty$.
- Results converge to the flat plate for $a/b \to \infty$.

Mesh-less discretization of the 3D problem

Spectral discretization in the normal coordinate of the tensor form of the 3D equations gives a ODE system of the form

$$\mathbf{F}(\frac{\partial \mathbf{u}}{\partial \xi}, \frac{\partial \mathbf{u}}{\partial \eta}, \mathbf{u}, \boldsymbol{\xi}) = 0, \tag{20}$$

The *data dependency domain* for a given point is (locally) the cone including the projection of the locus of vector velocities at the point. If we advance the computation by layers, then arrangements $\{A_i\}$ and $\{B_i\}$ are admissible but the $\{C_i\}$ are not. The constraint becomes stronger as the aperture angle of the hodograph becomes wider.

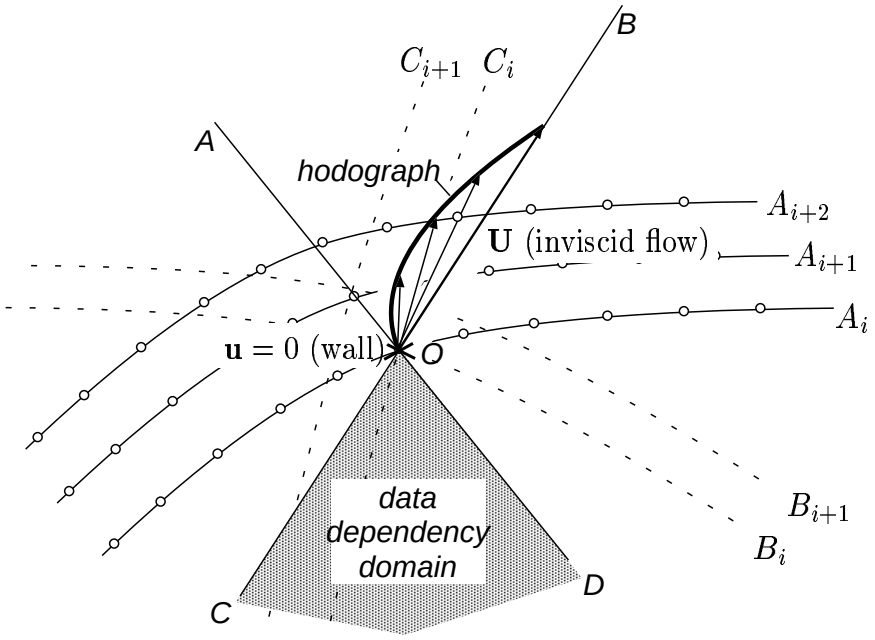

Figure 19: Data dependency domain(File: ../EPS/datadepend)

Mesh less discretization of the 3D problem *(continued...)*

In the neighborhood of the separation point the cone becomes 180° wide and the advancing front has to reach the separation line perfectly tangential to it. Otherwise, instabilities occur.

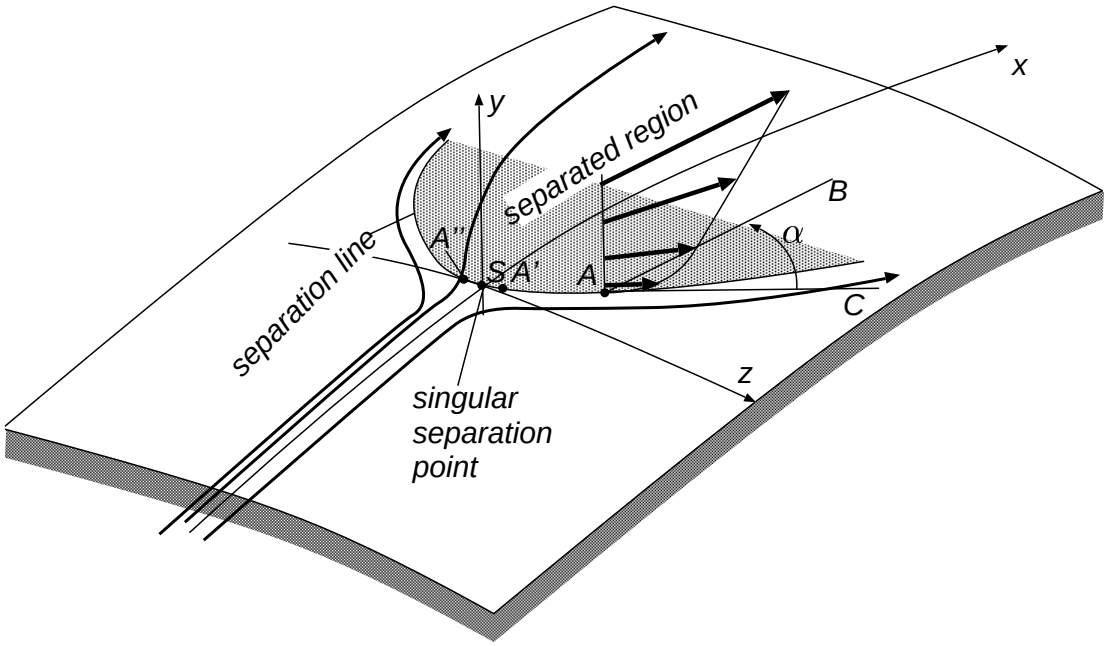

Figure 20: behavior of the data dependency domain near the separation line. (File: ../EPS/bubble)

Mesh less discretization of the 3D problem *(continued...)*

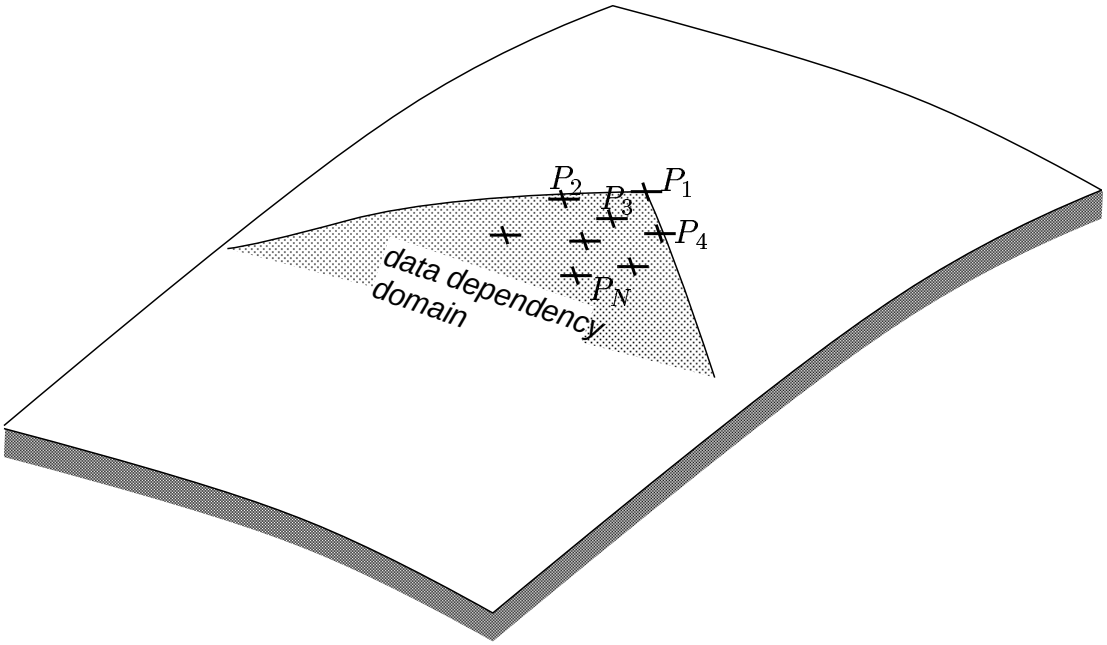

Figure 21: Stencil and data dependency domain for the boundary layer eqs. (File: ../EPS/meshless)

Compute coefficients for approximations to the first order derivatives by least-squares approximation,

$$\begin{aligned} \frac{\partial \phi}{\partial \xi} &\approx \sum_{j=1}^{N} c_j^{\xi}\, \phi_j, \\ \frac{\partial \phi}{\partial \eta} &\approx \sum_{j=1}^{N} c_j^{\eta}\, \phi_j. \end{aligned} \tag{21}$$

Then solve

$$\mathbf{F}\left(\sum_{j=1}^{N} c_j^{\xi}\, \mathbf{u}_j, \sum_{j=1}^{N} c_j^{\eta}\, \mathbf{u}_j, \mathbf{u}_j, \boldsymbol{\xi}_j \right) = \mathbf{0} \tag{22}$$

for $\mathbf{u}_1$.

3D Numerical results. Yawed circular cylinder

This case corresponds to a yawed cylinder such that the non-perturbed flow impinges at 45° to its axis (see figures 22 and 23). As indicates the theory, the velocity component normal to the axis of the cylinder is the same as for the non-yawed cylinder. However the limit streamlines, i.e. the streamlines for the fluid immediately over the wall) tend to curve near the separation point and to align with the separation streamline, which for cylinders is always an x =cnst curve. Here, the computations have been obtained with the potential velocity ($u = 2\sin(\phi)$) and separation occurs at the same point as for the non-yawed cylinder, i.e. at 104.45° which is in very good agreement with computations reported in the literature.

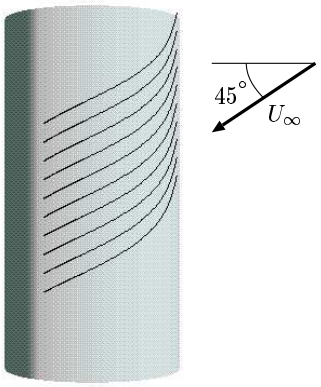

Figure 22: Inviscid streamlines.(File: ../EPS/cylindi)

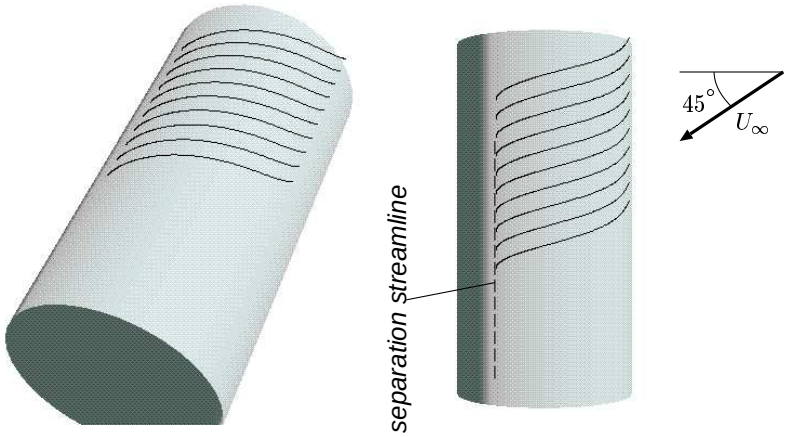

Figure 23: Computed viscous streamlines.(File: ../EPS/cylind)

3D Numerical results. Sphere

This is an axisymmetric flow without lateral (azimuthal) component of velocity. Using the velocity distribution given by the potential flow $U = 1.5\sin(\phi)$ we obtain the separation point at $\phi = 105.45^\circ$ which is in very good agreement with the value recommended by White as being between 104° and 106°.

Sphere (actual velocity distribution)

The actual velocity distribution can be approximated with very good precision as

$$\frac{U}{U_0} = 1.5(x/a) - 0.4371\,(x/a)^3 + 0.1481\,(x/a)^5 - 0.0423\,(x/a)^7 \quad (23)$$

With this velocity distribution the code predicts separation at $\phi = 81.6^\circ$ which is again in very good agreement with other computations and with the experimental value of 83° reported by Fage.

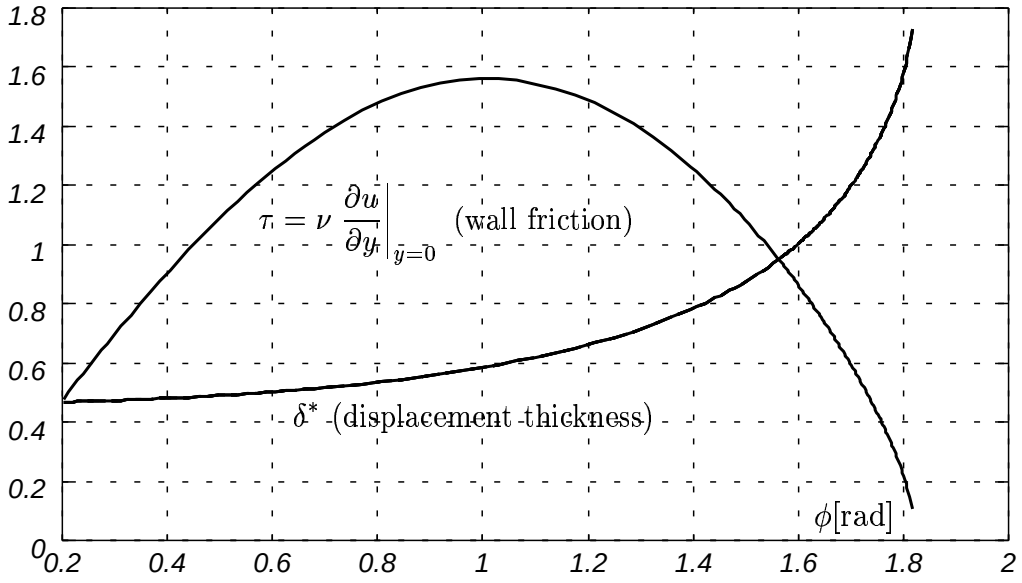

Figure 24: Results for the sphere with velocity distribution given by potential flow. (File: ../EPS/spherep)

3D Numerical results. Rotating sphere

In this case take the the actual distribution of velocity (23) but the sphere is rotating with an angular velocity $\omega R/U_\infty = 1$, about an axis parallel to the free stream velocity. Whereas the inviscid streamlines are simply meridians, the limit viscous streamlines have a tendency to rotate with the sphere, until they align with the separation streamline that is a parallel at 84.2° with respect to the pole facing the fluid. Note that rotation tends to stabilize the boundary layer against separation, resulting in a delay of almost 3 degrees. This is due to the centrifugal force that can be assimilated to a pressure gradient directed to the equator. Since the separation for the sphere happens before the equator this is equivalent to a favorable pressure gradient. This has a significant incidence in the drag also.

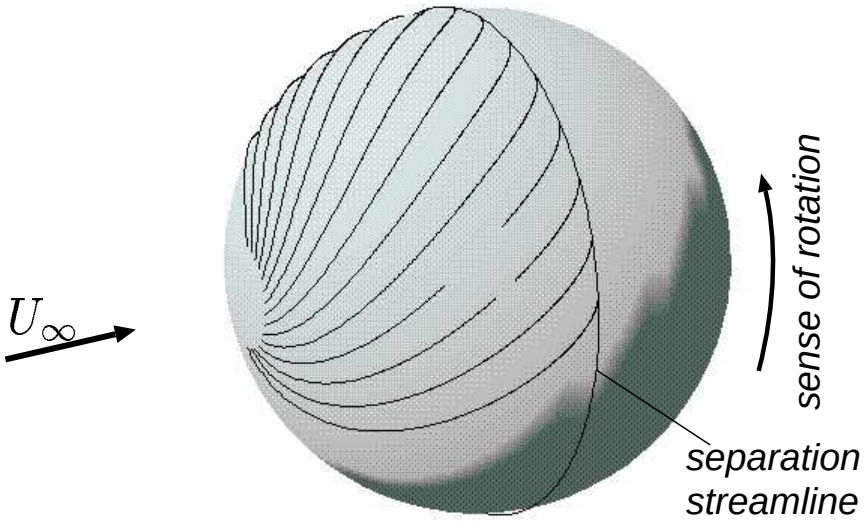

Figure 25: Limit streamlines for the rotating sphere. (File: ../EPS/rotsphere)

Conclusions

A spectrally accurate algorithm for the solution of the boundary layer equations with automatic scaling of the normal coordinate is presented. The scaling amounts to assume the scaling length as a further unknown and adding the corresponding restriction as a constraint. The resulting system of Differential-Algebraic Equations (DAE) is solved by eliminating one parameter in the expansion and solving the resulting system of ODE's. The spectral approximation is based on a direct mapping from the semi-infinite domain to a periodic problem and using a Fourier expansion, instead of truncating the semi-infinite domain and mapping to a bounded interval and using a Tchebyschev expansion. Several numerical results are presented, and spectral convergence is demonstrated by analysis of the decay rate of the coefficients in the expansion for similar flows, and by straightforward computation of the maximum error in the longitudinal velocity profile for the special case of flow towards a sink, for which an analytic expression is available. Also, the accuracy of the method when very few parameters are used was analyzed, by comparison with von Kármán and Pohlhausen's method.